













GLADE+: An Extended Galaxy Catalogue for Multimessenger Searches with Advanced Gravitational-wave Detectors

G. Dályá^{1,2} , R. Díaz¹, F. R. Bouchet³ , Z. Frei^{1,4} , J. Jasche⁵ ,
G. Lavaux³ , R. Macas⁶ , S. Mukherjee⁷ , M. Pálfi¹ , R. S. de Souza⁸ ,
B. D. Wandelt^{3,9,10} , M. Bilicki¹¹  and P. Raffai^{1,4} 

¹*Institute of Physics, Eötvös Loránd University, 1117 Budapest, Hungary*

²*Université Gent, B-9000 Ghent, Belgium*

³*Institut d'Astrophysique de Paris, UMR 7095, CNRS, Sorbonne Université, 98bis Boulevard Arago, 75014 Paris, France*

⁴*MTA-ELTE Astrophysics Research Group, 1117 Budapest, Hungary*

⁵*The Oskar Klein Centre, Department of Physics, Stockholm University, AlbaNova University Centre, SE 106 91 Stockholm, Sweden*

⁶*University of Portsmouth, Institute of Cosmology and Gravitation, Portsmouth PO1 3FX, United Kingdom*

⁷*Perimeter Institute for Theoretical Physics, 31 Caroline Street N., Waterloo, Ontario, N2L 2Y5, Canada*

⁸*Key Laboratory for Research in Galaxies and Cosmology, Shanghai Astronomical Observatory, Chinese Academy of Sciences, 80 Nandan Rd., Shanghai 200030, China*

⁹*Sorbonne Université, Institut Lagrange de Paris, 98 bis Boulevard Arago, 75014 Paris, France*

¹⁰*Center for Computational Astrophysics, Flatiron Institute, 162 5th Avenue, 10010, New York, NY, USA*

¹¹*Center for Theoretical Physics, Polish Academy of Sciences, al. Lotników 32/46, 02-668 Warsaw, Poland*

Accepted XXX. Received YYY; in original form ZZZ

ABSTRACT

We present GLADE+, an extended version of the GLADE galaxy catalogue introduced in our previous paper for multimessenger searches with advanced gravitational-wave detectors. GLADE+ combines data from six separate but not independent astronomical catalogues: the GWGC, 2MPZ, 2MASS XSC, HyperLEDA, and WISExSCOSPZ galaxy catalogues, and the SDSS-DR16Q quasar catalogue. To allow corrections of CMB-frame redshifts for peculiar motions, we calculated peculiar velocities along with their standard deviations of all galaxies having *B*-band magnitude data within redshift $z = 0.05$ using the "Bayesian Origin Reconstruction from Galaxies" formalism. GLADE+ is complete up to luminosity distance $d_L = 47^{+4}_{-2}$ Mpc in terms of the cumulative *B*-band luminosity of galaxies, and contains all of the brightest galaxies giving half of the total *B*-band luminosity up to $d_L \simeq 250$ Mpc. We include estimations of stellar masses and individual binary neutron star merger rates for galaxies with *W1* magnitudes in GLADE+. These parameters can help in ranking galaxies in a given gravitational wave localization volume in terms of their likelihood of being hosts, thereby possibly reducing the number of pointings and total integration time needed to find the electromagnetic counterpart.

Key words: catalogues — galaxies: distances and redshifts.

1 INTRODUCTION

During their third observing run (O3), the network of advanced gravitational-wave (GW) detectors consisting of the two interferometers of Advanced LIGO (Aasi et al. 2015), Advanced Virgo (Acernese et al. 2014), and the recently joined KAGRA (Akutsu et al. 2020) issued tens of prompt public alerts of significant GW events to allow for follow-up observations with electromagnetic (EM) and neutrino observatories (LIGO Scientific Collaboration & Virgo Collaboration 2020; Abbott et al. 2019b). Each alert includes the posterior probability distribution of the source sky position, for which the 90 percent credible localisation area is typically a few hundred square degrees (Abbott et al. 2018). For compact binary coalescence (CBC) events, luminosity distances can also be inferred, and thus full 3D sky localisation maps are released (Abbott et al. 2019b). Such events include suspected binary neutron star (BNS) mergers, which are the

leading candidates for joint GW+EM observations (see e.g. Abbott et al. 2017b).

An effective and typical way to find an EM counterpart for a GW event is to target a ranked set of potential host galaxies within the 3D localisation volume with follow-up telescope observations, and to look for variations between time-separated images of them (Abadie et al. 2012; Hanna et al. 2014; Fan et al. 2014; Gehrels et al. 2016). Besides telescope-dependent technical considerations and the probability distribution of the source location, one can also take into account astrophysically motivated factors in the ranking of host candidates. For example when dealing with a BNS merger event, one can sort host galaxy candidates by a model-based estimation of the BNS merger rate in them, which is expected to correlate with the star formation rate (Phinney 1991) (and thus with the blue luminosity, see e.g. Baret et al. 2012) and/or with the stellar mass (Artale et al. 2019, 2020) of the galaxy. In the favourable case of identifying the

host galaxy of a GW event through observing its EM counterpart (see e.g. [Abbott et al. 2017c](#)), one can refine the parameter estimations for the GW source with priors derived from the EM counterpart and properties of the host (see e.g. [Guidorzi et al. 2017](#); [Gao et al. 2017](#); [Abbott et al. 2019a](#)), or use GW parameter estimations to draw conclusions on the EM source (e.g. [Rezzolla et al. 2018](#)), the host (e.g. [Adhikari et al. 2020](#)), or on cosmological parameters including the Hubble constant (see [Abbott et al. 2017a](#)). Host galaxy candidates associated to detected CBC events can also be utilized in dark siren measurements of the Hubble constant when no EM counterpart of one or more CBC GW events is found ([Fishbach et al. 2019](#); [Soares-Santos et al. 2019](#)), in mapping out the expansion history ([Mukherjee & Wandelt 2018](#); [Mukherjee et al. 2021a](#); [Bera et al. 2020](#); [Diaz & Mukherjee 2021](#)), and in testing the general theory of relativity based on GW propagation ([Mukherjee et al. 2020, 2021b](#)).

In [Dálya et al. \(2018\)](#), we introduced the *Galaxy List for the Advanced Detector Era* (GLADE) value-added full-sky catalogue of galaxies ([Dálya et al. 2016](#)), which since then has extensively been used by the LIGO-Virgo Collaboration ([Abbott et al. 2017a, 2020, 2021a,b](#)) and others (see [Dálya et al. 2018](#) for references, and e.g. [Lundquist et al. 2019](#); [Antier et al. 2020](#); [Gompertz et al. 2020](#); [Keivani et al. 2021](#); [Paterson et al. 2021](#); [Sasada et al. 2021](#); [Fishbach et al. 2019](#); [Finke et al. 2021](#)) for the purposes mentioned above. Additionally, GLADE has been integrated into tools supporting optimal selections of target galaxies for follow-up observations ([Rana & Mooley 2019](#); [Coughlin et al. 2019](#); [Salmon et al. 2020](#); [Wyatt et al. 2020](#); [Xu et al. 2020](#)), and was used for identifying or extracting information on potential hosts of fast radio bursts (see e.g. [CHIME/FRB Collaboration et al. 2019](#)), short gamma-ray bursts (see e.g. [Dichiara et al. 2020](#)), supernova shock breakouts ([Alp & Larsson 2020](#)), and other transient phenomena observed in X-ray ([Caglar & Hudaverdi 2017](#)), optical (see e.g. [Andrew et al. 2021](#); [Killestein et al. 2021](#)), and radio bands (see e.g. [Riseley et al. 2017](#); [Kuiack et al. 2021](#)).

In this paper, we introduce an updated, extended, and improved version of GLADE, which we will refer to as GLADE+. GLADE+ contains ~ 22.5 million galaxies and ~ 750 thousand quasars (compared to ~ 3 million galaxies and ~ 300 thousand quasars in GLADE) as a result of cross-matching GLADE with the WISE \times SuperCOSMOS Photometric Redshift Catalogue (WISE \times SCOSPZ) and updating the quasar database of GLADE with the SDSS-DR16Q quasar catalogue. To allow corrections of CMB-frame redshifts for peculiar motions, we calculated peculiar velocities along with their standard deviations of all galaxies having B -band magnitude data within redshift $z = 0.05$ using the "Bayesian Origin Reconstruction from Galaxies" formalism ([Mukherjee et al. 2021c](#)). We estimated stellar masses and binary neutron star merger rates with all GLADE+ galaxies with $W1$ -band magnitude data and included these in the catalogue. The aim of these improvements is to continue serving the purposes mentioned above and potentially serve new ones, especially in light of the ongoing preparations for the fourth observing run of the LIGO-Virgo-KAGRA network scheduled for 2022 ([Abbott et al. 2018](#)).

This paper is organized as follows. In Section 2 we introduce the catalogues and methods we used to create GLADE+, including the peculiar velocity correction and the stellar mass and binary neutron star merger rate estimations. In Section 3 we quantify the completeness of GLADE+ based on the measured B - and K_s -band luminosities of GLADE+ galaxies. In Section 4 we describe the exact format of the catalogue and in Section 5 we draw our conclusions.

Throughout this paper we adopt a flat Λ CDM cosmology with the following parameters from the Planck 2018 results: $H_0 = 100h = 67.66 \text{ km s}^{-1} \text{ Mpc}^{-1}$, $\Omega_M = 0.3111$ and $\Omega_\Lambda = 0.6889$ ([Planck Collaboration et al. 2020](#)).

2 CONSTRUCTION OF THE GLADE+ CATALOGUE

We have constructed GLADE+ from six separate but not independent astronomical catalogues: the Gravitational Wave Galaxy Catalogue¹ (GWGC, see [White et al. 2011](#)), HyperLEDA² ([Makarov et al. 2014](#)), the 2 Micron All-Sky Survey Extended Source Catalog³ (2MASS XSC, see [Jarrett et al. 2000](#) and [Skrutskie et al. 2006](#)), the 2MASS Photometric Redshift Catalog⁴ (2MPZ, see [Bilicki et al. 2014](#)), the WISE \times SCOSPZ Photometric Redshift Catalogue⁵ (WISE \times SCOSPZ, see [Bilicki et al. 2016a](#)), and the Sloan Digital Sky Survey quasar catalogue from the 16th data release⁶ (SDSS-DR16Q, see [Lyke et al. 2020](#)). As we have used the first four of these catalogues in creating the GLADE galaxy catalogue, the relevant characteristics of these are summarized in [Dálya et al. \(2018\)](#). In Section 2.1 we only describe the WISE \times SCOSPZ and SDSS-DR16Q catalogues, and discuss the cross-matching between GLADE and WISE \times SCOSPZ, as well as the results we obtained. In Section 2.2 we describe the method we used for estimating peculiar velocities, and in Section 2.3 we introduce the methods used to estimate the stellar masses of and BNS merger rates in the individual galaxies.

2.1 Cross-matching

The WISE \times SCOSPZ catalogue was constructed by cross-matching the AllWISE full-sky release ([Cutri et al. 2014](#)) of the Wide-field Infrared Survey Explorer (WISE, see [Wright et al. 2010](#)), which is the most comprehensive survey of the mid-infrared sky, and the SuperCOSMOS Sky Survey ([Hambly et al. 2001](#)), the result of an automated scanning and digitizing of photographic plates from the United Kingdom Schmidt Telescope and the Palomar Observatory Sky Survey-II. WISE \times SCOSPZ contains ~ 20 million galaxies with photometric redshifts calculated using an artificial neural network algorithm ([Collister & Lahav 2004](#)). The redshifts have errors nearly independent of distance, with an overall accuracy of $\sigma_z/(1+z) \simeq 0.033$ ([Bilicki et al. 2016a](#)). The catalogue contains magnitude information in the B_J and R_F bands from SuperCOSMOS ([Peacock et al. 2016](#)) and in the $W1$ and $W2$ WISE bands. In order to calculate the magnitudes of the galaxies in the Johnson-Cousins B -band, we have used the color equations presented in [Peacock et al. \(2016\)](#).

We have created GLADE+ by cross-matching GLADE v2.4⁷ with the WISE \times SCOSPZ catalogue and then replacing the quasars with the newer set from SDSS-DR16Q and removing the globular clusters. We could not use the method described in [Dálya et al. \(2018\)](#) for cross-matching GLADE with WISE \times SCOSPZ, as duplicate galaxies could not simply be found by their designations. Hence we used a resolution of 2 arcseconds, i.e. if a WISE \times SCOSPZ galaxy lied closer to a GLADE galaxy than this threshold, we treated them as being the same object and merged them. This distance threshold was motivated by the fact that 2 arcseconds is the maximal resolution in the WISE \times SCOSPZ catalogue and false positive associations start to dominate above this value. The order of magnitude of the threshold is also consistent with that of previous GLADE cross-matches, note however that in previous applications we could take other parameters

¹ <http://vizier.u-strasbg.fr/viz-bin/VizieR?-source=GWGC>

² <http://leda.univ-lyon1.fr/>

³ <https://old.ipac.caltech.edu/2mass/>

⁴ <http://ssa.roe.ac.uk/TWOMPZ.html>

⁵ <http://ssa.roe.ac.uk/WISExSCOS.html>

⁶ https://www.sdss.org/dr16/algorithms/qso_catalog/

⁷ The specifics of different GLADE versions are described on the GLADE website: <http://glade.elte.hu>

of the galaxies into account as well, such as luminosity distances and B magnitudes (Dálya et al. 2018).

The GLADE+ catalogue incorporated the SDSS-DR12Q quasar catalogue, which, in GLADE+, we replaced entirely with the more recent and extended SDSS-DR16Q catalogue. This catalogue contains data for $\sim 750,000$ quasars (including the $\sim 300,000$ quasars published in SDSS-DR12Q), which makes it the largest selection of spectroscopically confirmed quasars to date.

Cross-matching and updating the catalogues resulted in the GLADE+ catalogue containing 23,181,758 objects from which 22,431,348 are galaxies and 750,410 are quasars. The sky distribution of GLADE+ objects are shown in Figure 1 as a density plot. The plane of the Milky Way is clearly noticeable in the figure, as the gas and dust reduces the visibility towards those directions and different sky surveys used various cuts in galactic latitude. Other anisotropies are arising from the different sensitivities and footprints of the various sky surveys.

Due to incorporating the WISExSCOSPZ catalogue, 21,165,400 sources in GLADE+ had $W1$ magnitudes available from that sample, which we have used to estimate their stellar masses and binary neutron star merger rates, see Section 2.3. In order to supplement as many of the remaining ones with $W1$ as possible, we first cross-matched them with AllWISE, using 3 arcsecond matching radius and keeping only the closest matches. We found a match for over 1.76 million galaxies, which left us with $\sim 260,000$ without a WISE counterpart. For part of the latter (32,153 galaxies) we provide $W1$ apparent magnitude estimates based on K_s -band measurements available in 2MASS. To obtain these estimates, we first fitted the mean $W1 - K_s$ colour as a function of redshift for sources with available spectroscopic redshifts, K_s and $W1$ magnitudes in the 2MPZ catalogue. This effective $W1 - K_s$ colour relation is then added to the K_s band measurements for those sources in GLADE+ which have K_s magnitudes from 2MASS but do not have the $W1$ one, to obtain the $W1$ magnitude estimate.

2.2 Peculiar velocity correction

The correction of peculiar velocity for the low redshift galaxies is essential to correctly calculate the true redshift. The estimation of peculiar velocities for galaxies in GLADE+ is made using the method proposed by Mukherjee et al. (2021c), which relies on a Bayesian formalism called "Bayesian Origin Reconstruction from Galaxies" (BORG). The BORG forward modelling method infers a probabilistic and physically plausible model of the three-dimensional cosmic matter distribution from observed galaxies in cosmological surveys to derive the linear and partially the non-linear component of the velocity field (see e.g. Jasche & Wandelt 2013; Jasche et al. 2015; Lavaux & Jasche 2016; Jasche & Lavaux 2019). This method solves a large-scale Bayesian inverse problem by fitting a dynamical structure formation model to data, and estimates the initial conditions of the early Universe from which presently-observed structures can be explained. The BORG algorithm marginalizes over unknown galaxy bias and accounts for selection and evolutionary effects while providing the velocity field as part of the dynamical model. The reliability of this method is verified with an N -body simulation to check the consistency of the velocity fields provided by the posterior distributions sampled by BORG and the one provided by the original N -body simulation (Mukherjee et al. 2021c). This method gives a set of points in the parameter space (a spatial grid of 256^3 values with a spatial resolution of $2.64 \text{ Mpc } h^{-1}$ for the initial conditions plus the bias parameters) that provides a numerical approximation of the posterior distribution of these parameters given the observed large scale struc-

ture observation. For each sample of the posterior, initial and final positions of the dark matter particles are provided, from which the velocity field can be estimated using the Simplex-in-Cell estimator (SIC, Hahn et al. 2015; Leclercq et al. 2017). More details on this method and its validation can be found in Mukherjee et al. (2021c).

Along with the velocity estimation from BORG, we also include the contribution from the non-linear virial component of the velocity field. The radial components of the virial velocities are modelled as Gaussian random variates with variance (Sheth & Diaferio 2001; Mukherjee et al. 2021c)

$$\sigma_{\text{vir}} = 476 g_v (\Delta_{\text{nl}}(z)E(z)^2)^{1/6} \left(\frac{M_h}{10^{15} M_\odot h^{-1}} \right)^{1/3}, \quad (1)$$

where $g_v = 0.9$, $\Delta_{\text{nl}}(z) = 18\pi^2 + 60x - 32x^2$, h is the reduced Hubble constant, and $x = \Omega_m(1+z)^3/E^2(z) - 1$; $E(z)$ is the cosmological expansion function. In order to use this relation, we need to estimate the halo mass M_h . We have used a mass-luminosity relation (Vale & Ostriker 2004)

$$L_B = \frac{A(M_h/M_r)^b}{[c + (M_h/M_r)^{dk}]^{1/k}}, \quad (2)$$

where $A = 5.7 \times 10^9$, $M_r = 10^{11} M_\odot$, $b = 4$, $c = 0.57$, $d = 3.72$, and $k = 0.23$, to estimate the mass from the B -band luminosity L_B of the galaxy. The total variance in the velocity field is then calculated as $\sigma_{\text{tot}}^2 = \sigma_{\text{BORG}}^2 + \sigma_{\text{vir}}^2$.

Using this method we have estimated the mean value⁸ of the velocity field to all GLADE+ galaxies which cross-match with the 2M++ compilation (Lavaux & Hudson 2011; Mukherjee et al. 2021c) for galaxies up to redshift $z = 0.05$ for which the B -band luminosity is available, along with the standard deviation σ_{tot} of the peculiar velocity which includes both linear and non-linear components of the velocity field. The conversion from the heliocentric redshift to the CMB-frame redshift are performed using the observation of the CMB temperature anisotropy by FIRAS (Fixsen et al. 1996). The uncertainty in the velocity error is translated into an uncertainty in the redshift and is provided in the catalog.

2.3 Stellar mass and binary neutron star merger rate estimations

According to Artale et al. (2019) stellar masses (i.e. the total mass of the living and remnant stars) of galaxies strongly correlate with the merger rates of the colliding binaries. These parameters can help in ranking the galaxies in a GW localization volume, thereby possibly reducing the number of pointings and the total integration time needed to find the EM counterpart. The stellar mass is also one of the key parameters of the formation and evolution of galaxies (e.g. van Loon et al. 2021; Ahad et al. 2021; Engler et al. 2020). Hence we aimed to estimate stellar masses and merger rates for as many galaxies in GLADE+ as we can.

To estimate the stellar mass of a galaxy the so-called (stellar) mass-to-light ratio (M_*/L) is required that can be obtained from stellar population synthesis models. Then the estimation can be performed with spectral energy distribution fitting or based on one or more magnitude bands or colours (see Courteau et al. 2014 for a review). Since only a few magnitude bands (B and some infrared)

⁸ The direction of the velocity field is chosen such that the positive value of the velocity field indicates that the object is moving away from us.

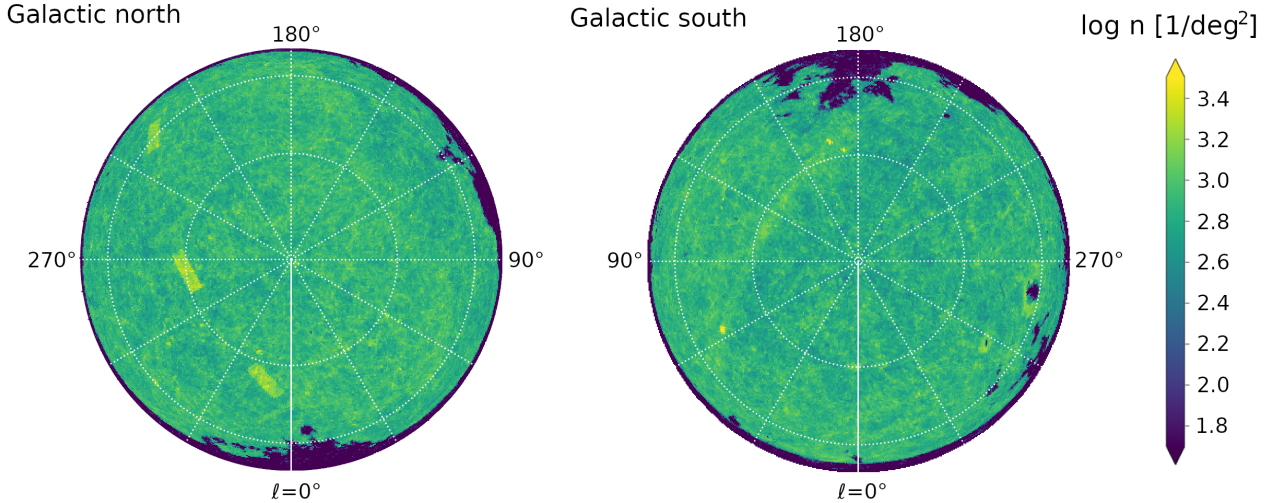


Figure 1. The base-10 logarithm of the number density (n) of objects in GLADE+ using azimuthal projection with galactic coordinates. The plane of the Milky Way obscures the visibility of background galaxies, hence the (blue) underdense regions at the edges of the plots. Overdense (yellow) patches and stripes originating from the HyperLEDA catalogue show up as a result of deeper, more sensitive surveys (such as SDSS and GAMA), that have been made towards the corresponding sky locations.

are contained in the GLADE+ catalogue, and no spectral energy distributions are available, it is straightforward to use one of the magnitude-based stellar mass estimation methods. The mid-infrared M_*/L is relatively insensitive to the different stellar populations, particularly in the absence of ongoing star formation, and in addition it is not very sensitive to dust attenuation (see e.g. [Wen et al. 2013](#); [Röck et al. 2015](#)). Therefore we estimated the stellar mass based on the mid-infrared WISE magnitudes.

According to [Kettlety et al. \(2018\)](#) the mass-to-light ratio in the $W1$ -band is

$$M_*/L_{W1} = 0.65 \pm 0.07, \quad (3)$$

for passive galaxies, which the authors claim can provide at least as accurate mass estimates for galaxies with redshifts $z \leq 0.15$ as more complex methods. We calculated the stellar mass according to this equation for galaxies having WISE $W1$ magnitude. The $W1$ luminosity can be calculated as

$$L_{W1}(L_\odot) = 10^{-0.4(M-M_\odot)}, \quad (4)$$

here $M_\odot = 3.24^m$ is the $W1$ magnitude of the Sun and

$$M = m + 5 - 5 \log_{10} d_L - K \quad (5)$$

is the absolute magnitude of the source in the $W1$ -band, where m is the apparent $W1$ magnitude, d_L is the luminosity distance and

$$K = -7.1 \log_{10}(1+z) \quad (6)$$

is the K correction of [Kettlety et al. \(2018\)](#), where z is the heliocentric redshift. We do not apply correction for extinction because WISE magnitudes are already corrected ([Bilicki et al. 2016b](#)). We accepted stellar masses larger than $10^5 M_\odot$ as this value is the lower limit of the stellar mass of dwarf galaxies (e.g. [Garrison-Kimmel et al. 2019](#)). We could estimate the stellar mass of 21,779,151 (~ 94 percent) of the galaxies in GLADE+.

We also provide the error of the stellar mass of each galaxy using the propagation of uncertainty, where we took into account the correlation terms. The errors of the luminosity distance were calculated from the error of redshift in the cases where it is not known. When

the error of the $W1$ magnitude was not known for individual galaxies, we calculated with the mean $W1$ error from WISExSCOSPZ. We find that the mean relative stellar mass error is 46 percent, while the median is 37 percent. The stellar mass values in the catalogue are rounded with respect to the errors. The codes of the stellar mass estimation are publicly available on the GLADE website.

The binary neutron star merger rates (n_{GW}) can be calculated from the stellar mass values according to [Artale et al. \(2019\)](#):

$$\log_{10}(n_{GW}/\text{Gyr}) = (1.15 \pm 0.08) \log_{10}(M_*[M_\odot]) - (7.22 \pm 0.22), \quad (7)$$

which is valid below $z \leq 0.1$ and they studied galaxies with stellar masses $M_* > 10^7 M_\odot$, so we calculated the merger rate for galaxies satisfying these conditions. Applying these criteria resulted in 3,083,920 galaxies with binary neutron star merger rates. In addition, [Artale et al. \(2019\)](#) provides equations for the merger rate of binary black holes:

$$\log_{10}(n_{GW}/\text{Gyr}) = (0.80 \pm 0.07) \log_{10}(M_*[M_\odot]) - (4.14 \pm 0.19), \quad (8)$$

and black hole - neutron star pairs as well:

$$\log_{10}(n_{GW}/\text{Gyr}) = (0.87 \pm 0.08) \log_{10}(M_*[M_\odot]) - (4.99 \pm 0.22). \quad (9)$$

Note, that we only provide merger rates for BNSs in GLADE+, however using the stellar masses from the catalogue and Equations 8-9 the binary black hole and the black hole - neutron star merger rates can be calculated as well.

3 CATALOGUE COMPLETENESS

Following the methods we introduced in [Dályá et al. \(2018\)](#), we quantify the completeness of GLADE+ using two different methods:

(i) by comparing, within different luminosity distance limits, the integrated B luminosity of GLADE+ galaxies to calculated reference values (see details in next paragraphs), and (ii) by comparing luminosity distributions of GLADE+ galaxies to the Schechter function within different luminosity distance shells.

The first method was originally used by White et al. (2011) to calculate the completeness of the GWGC catalog. Here we compare the integrated B -band luminosity of GLADE+ galaxies within different luminosity distance limits to the total B -band luminosity we would expect from the same volume given a complete catalogue of homogeneously distributed galaxies with B -band luminosity density $(1.98 \pm 0.16) \times 10^{-2} L_{10} \text{ Mpc}^{-3}$, where $L_{10} = 10^{10} L_{B,\odot}$ and $L_{B,\odot}$ is the solar luminosity in the B -band. Figure 2 shows a comparison between the completeness values inferred using this method for the GLADE+ catalogue and its constituent catalogues, GLADE v2.4 and WISEXSCOSPZ. Completeness values over 100 percent are results of local overdensities of galaxies. The drop in completeness around a luminosity distance of 220 Mpc corresponds to the limit we used for the peculiar velocity correction (see Section 2.2). As we can see from the figure, most of the completeness below ~ 330 Mpc comes from the GLADE v2.4 catalogue and above this distance the contributions from WISEXSCOSPZ galaxies start to dominate. Based on this completeness measure, GLADE+ is complete up to $d_L = 47_{-2}^{+4}$ Mpc. GLADE+ has a completeness of ~ 55 percent within the single-detector LIGO Livingston BNS range during O3 (130 Mpc) and ~ 45 percent within the maximal planned single-detector BNS range in O4 (190 Mpc, see Abbott et al. 2018).

We have also used a second method to characterize the completeness of GLADE+. Here we divided the galaxies into 12 luminosity distance shells each having a width of $\Delta d_L = 16.7$ Mpc. We have constructed histograms of B and K_s band luminosities of the GLADE+ galaxies for each shell, which we show in Figure 3 together with their corresponding Schechter functions. For the B -band Schechter function we have used the following values from Gehrels et al. (2016): $\phi^* = 1.6 \times 10^{-2} h^3 \text{ Mpc}^{-3}$, $M_B^* = -20.47$ and $a = -1.07$. For the K_s -band Schechter function we have used the following parameters from Kochanek et al. (2001): $\phi^* = 1.16 \times 10^{-2} h^3 \text{ Mpc}^{-3}$, $M_K^* = -23.39$ and $a = -1.09$. Figure 3 shows that as distance increases, more and more faint galaxies are missing from GLADE+ in both bands. We can also see that the faint limit of our catalogue decreases more rapidly in the K_s -band.

Following Gehrels et al. (2016) we have compared the integrated luminosity of the brighter subset of galaxies giving half of the total luminosity in each shell to the expected value corresponding to the Schechter function. In this analysis we have extended the luminosity distance limit to $d_L = 500$ Mpc and the bin size to $\Delta d_L = 20$ Mpc. The completeness of GLADE+ in the B and K_s -bands in the different bins is shown in Figure 4. The figure shows that the completeness for the brighter subset of galaxies decreases less rapidly in the K_s -band over $d_L \approx 100$ Mpc, and using this definition the catalogue is complete in the B -band up to ~ 250 Mpc and up to ~ 390 Mpc in the K_s band. Note, that we have considered only the brighter half of all the galaxies for this analysis, so even if the completeness is 100 percent or above at a given distance, GLADE+ can still lack a large number of faint galaxies there.

4 DESCRIPTION OF THE GLADE+ CATALOGUE

The GLADE+ catalogue is available as a txt file on the GLADE website⁹. Columns of each line of the file contain the following data (where available) for each GLADE+ object:

- 1 GLADE+ catalogue number
- 2 Principal Galaxies Catalogue number
- 3 Name in the GWGC catalogue
- 4 Name in the HyperLEDA catalogue
- 5 Name in the 2MASS XSC catalogue
- 6 Name in the WISEXSuperCOSMOS catalogue (wiseX)
- 7 Name in the SDSS-DR16Q catalogue
- 8 Object type flag: 'Q' means that the source is from the SDSS-DR16Q catalogue, 'G' means that it is from another catalogue and has not been identified as a quasar
- 9 Right ascension in degrees
- 10 Declination in degrees
- 11 Apparent B magnitude
- 12 Absolute error of apparent B magnitude
- 13 B magnitude flag: '0' if the B magnitude is measured, '1' if it is calculated from the B_J magnitude
- 14 Absolute B magnitude
- 15 Apparent J magnitude
- 16 Absolute error of apparent J magnitude
- 17 Apparent H magnitude
- 18 Absolute error of apparent H magnitude
- 19 Apparent K_s magnitude
- 20 Absolute error of apparent K_s magnitude
- 21 Apparent $W1$ magnitude
- 22 Absolute error of apparent $W1$ magnitude
- 23 Apparent $W2$ magnitude
- 24 Absolute error of apparent $W2$ magnitude
- 25 $W1$ flag: '0' if the $W1$ magnitude is measured, '1' if it is calculated from the K_s magnitude
- 26 Apparent B_J magnitude
- 27 Absolute error of apparent B_J magnitude
- 28 Redshift in the heliocentric frame
- 29 Redshift converted to the Cosmic Microwave Background (CMB) frame
- 30 Redshift correction flag: '0' if the CMB frame redshift and luminosity distance values given in columns 25 and 28 are not corrected for the peculiar velocity, '1' if they are corrected values
- 31 Error of redshift from the peculiar velocity estimation
- 32 Measurement error of heliocentric redshift
- 33 Luminosity distance in Mpc units
- 34 Error of luminosity distance in Mpc units
- 35 Redshift and luminosity distance measurement flag: '0' if the galaxy has no measured redshift or distance value, '1' if it has a measured photometric redshift from which we have calculated its luminosity distance, '2' if it has a measured luminosity distance value from which we have calculated its redshift, '3' if it has a measured spectroscopic redshift from which we have calculated its luminosity distance
- 36 Stellar mass in $10^{10} M_\odot$ units
- 37 Absolute error of stellar mass in $10^{10} M_\odot$ units
- 38 Base-10 logarithm of estimated BNS merger rate in the galaxy in Gyr^{-1} units
- 39 Absolute error of estimated BNS merger rate in the galaxy

⁹ GLADE website: <http://glade.elte.hu>

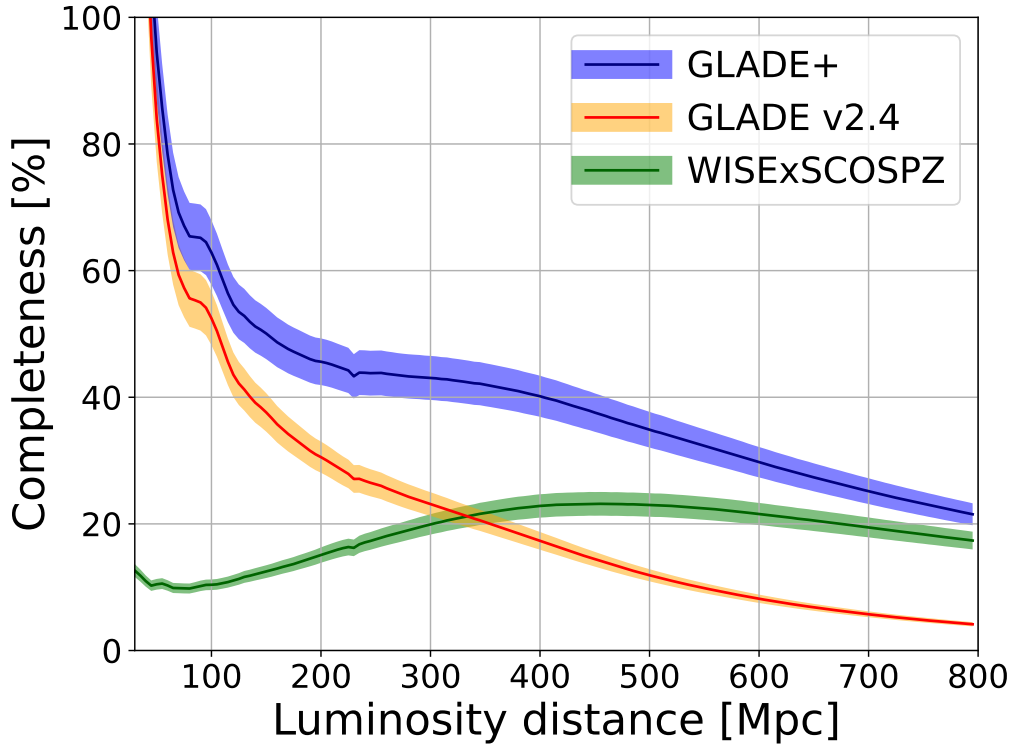


Figure 2. The completeness in terms of the normalized integrated B -band luminosity of galaxies in GLADE+ (blue) and its constituent catalogues (i.e. GLADE v2.4 shown in orange and WISExSCOSPZ shown in green) within luminosity distances indicated on the x -axis. The normalization is carried out with the integrated B -band luminosity calculated from an average B -band luminosity density of a complete catalogue of homogeneously distributed galaxies (see Kopparapu et al. 2008 for details). The completeness value exceeds 100 percent within 47 Mpc due to a local overdensity of galaxies around the Milky Way. The completeness below ~ 330 Mpc is mostly due to the GLADE galaxies, and WISExSCOSPZ galaxies contribute more for distances larger than ~ 330 Mpc.

5 CONCLUSIONS

The GLADE+ galaxy catalogue is an extended version of the GLADE catalogue we have optimized for multimessenger searches with advanced GW detectors. It contains more than 23 million objects from which more than 22 million are galaxies and $\sim 750,000$ are quasars. As the effects of peculiar motions are important for nearby galaxies for both the EM follow-up and cosmological analyses, we have estimated the peculiar velocities along with their standard deviations for galaxies in GLADE+ with B -band magnitude data having redshifts $z \leq 0.05$ using the BORG forward modelling method. GLADE+ is complete up to $d_L = 47^{+4}_{-2}$ Mpc in terms of the cumulative B -band luminosity of galaxies, and contains all of the brightest galaxies giving half of the total B -band luminosity up to $d_L \approx 250$ Mpc.

As according to theoretical models the stellar mass of galaxies strongly correlates with the merger rate of colliding binaries, we have calculated the stellar masses and the BNS merger rates (together with their errors) of each galaxy having WISE magnitudes. These parameters can help to rank the galaxies in a given GW localization volume, thereby possibly reducing the number of pointings and the total integration time needed to find the EM counterpart.

ACKNOWLEDGEMENTS

This paper was reviewed by the LIGO Scientific Collaboration under LIGO Document P... . The authors would like to thank Simone Mastrogiovanni, Surhud More and John Peacock for fruitful discussions throughout the project. The authors thank Bence Bécsy

for useful comments on the manuscript. We are grateful for the Wide Field Astronomy Unit (WFAU) for providing the WISExSCOS and 2MPZ data used in creating GLADE+. We acknowledge the usage of the HyperLeda database (<http://leda.univ-lyon1.fr>). GD is supported through the ÚNKP-19-3 New National Excellence program of the Hungarian Ministry of Human Capacities and the iBOF-project BOF20/IBF/124. Research at Perimeter Institute is supported in part by the Government of Canada through the Department of Innovation, Science and Economic Development Canada and by the Province of Ontario through the Ministry of Colleges and Universities. The work of BDW is supported by the Labex ILP (reference ANR-10-LABX-63) part of the IDEX SUPER, received financial state aid managed by the Agence Nationale de la Recherche, as part of the programme Investissements d’avenir under the reference ANR-11-IDEX-0004-02. The Center for Computational Astrophysics is supported by the Simons Foundation. This work was supported by the ANR BIG4 project, grant ANR-16-CE23-0002 of the French Agence Nationale de la Recherche. A part of the analysis was carried out at the Horizon cluster hosted by Institut d’Astrophysique de Paris. We thank Stephane Rouberol for smoothly running the Horizon cluster. This work was granted access to the HPC resources of CINES (Centre Informatique National de l’Enseignement Supérieur) under the allocation A0020410153 made by GENCI. This work is done within the Aquila Consortium¹⁰. JJ acknowledges support by the Swedish Research Council (VR) under

¹⁰ <https://www.aquila-consortium.org/>

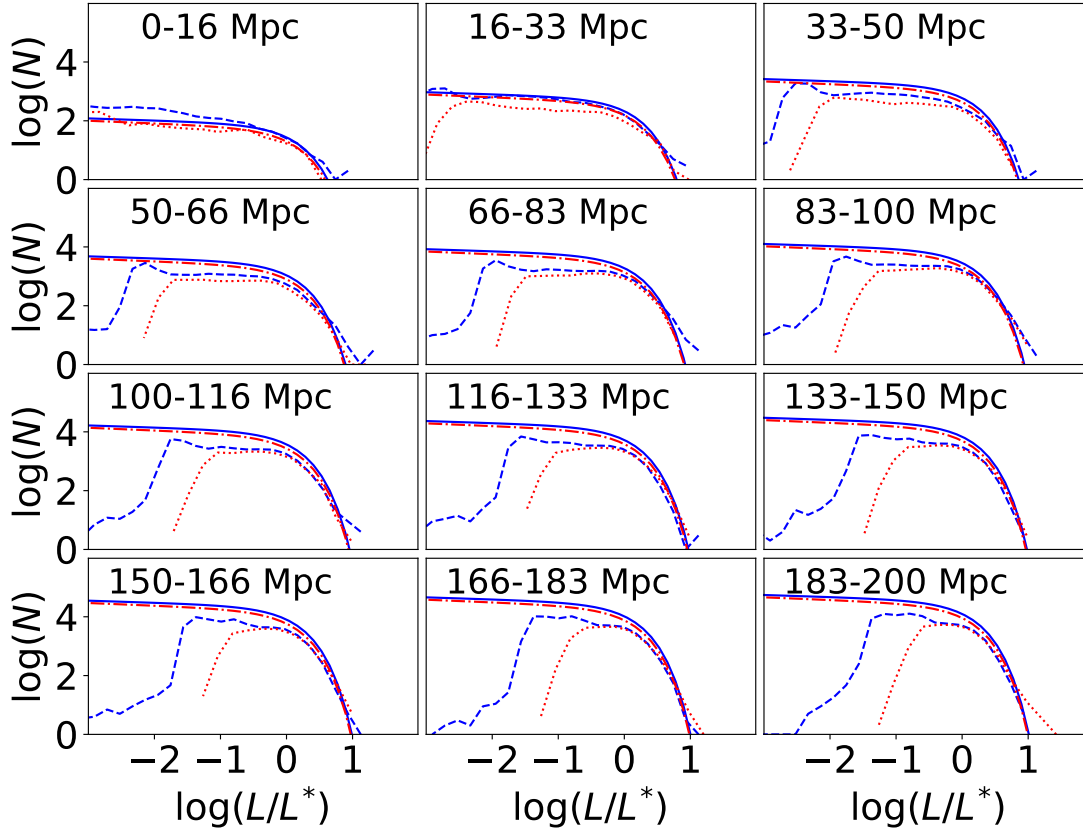


Figure 3. Luminosity histograms of GLADE+ galaxies within different luminosity distance shells in terms of their measured B -band and K_s -band luminosities (blue dashed and red dotted lines, respectively), compared to the same histograms we expect for complete catalogues based on B and K_s -band Schechter function measurements (blue solid and red dash-dotted lines, respectively). L^* is the characteristic luminosity of the Schechter function.

the project 2020-05143 – “Deciphering the Dynamics of Cosmic Structure”. We acknowledge the use of following packages in this analysis: Astropy (Astropy Collaboration et al. 2013, 2018), IPython (Pérez & Granger 2007), Matplotlib (Hunter 2007), NumPy (van der Walt et al. 2011), and SciPy (Jones et al. 2001).

REFERENCES

- Aasi J., et al., 2015, *Classical and Quantum Gravity*, 32, 074001
 Abadie J., et al., 2012, *A&A*, 539, A124
 Abbott B. P., et al., 2017a, *Nature*, 551, 85
 Abbott B. P., et al., 2017b, *The Astrophysical Journal*, 848, L12
 Abbott B. P., et al., 2017c, *ApJ*, 848, L12
 Abbott B. P., et al., 2018, *Living Reviews in Relativity*, 21, 3
 Abbott B. P., et al., 2019a, *Physical Review X*, 9, 011001
 Abbott B. P., et al., 2019b, *The Astrophysical Journal*, 875, 161
 Abbott R., et al., 2020, *ApJ*, 896, L44
 Abbott B. P., et al., 2021a, *ApJ*, 909, 218
 Abbott R., et al., 2021b, *ApJ*, 915, 86
 Acernese F., et al., 2014, *Classical and Quantum Gravity*, 32, 024001
 Adhikari S., Fishbach M., Holz D. E., Wechsler R. H., Fang Z., 2020, *ApJ*, 905, 21
 Ahad S. L., Bahé Y. M., Hoekstra H., van der Burg R. F. J., Muzzin A., 2021, *Monthly Notices of the Royal Astronomical Society*, 504, 1999
 Akutsu T., et al., 2020, Overview of KAGRA: Detector design and construction history ([arXiv:2005.05574](https://arxiv.org/abs/2005.05574))
 Alp D., Larsson J., 2020, *ApJ*, 896, 39
 Andrew S., Swihart S. J., Strader J., 2021, *ApJ*, 908, 180
 Antier S., et al., 2020, *MNRAS*, 492, 3904
 Artale M. C., Mapelli M., Giacobbo N., Sabha N. B., Spera M., Santoliquido F., Bressan A., 2019, *MNRAS*, 487, 1675
 Artale M. C., Mapelli M., Bouffanais Y., Giacobbo N., Pasquato M., Spera M., 2020, *MNRAS*, 491, 3419
 Astropy Collaboration et al., 2013, *A&A*, 558, A33
 Astropy Collaboration et al., 2018, *AJ*, 156, 123
 Baret B., et al., 2012, *Phys. Rev. D*, 85, 103004
 Bera S., Rana D., More S., Bose S., 2020, *Astrophys. J.*, 902, 79
 Bilicki M., Jarrett T. H., Peacock J. A., Cluver M. E., Steward L., 2014, *ApJS*, 210, 9
 Bilicki M., et al., 2016b, *The Astrophysical Journal Supplement Series*, 225, 5
 Bilicki M., et al., 2016a, *ApJS*, 225, 5
 CHIME/FRB Collaboration et al., 2019, *ApJ*, 885, L24
 Caglar T., Hudaverdi M., 2017, *MNRAS*, 471, 4990
 Collister A. A., Lahav O., 2004, *PASP*, 116, 345
 Coughlin M. W., et al., 2019, *MNRAS*, 489, 5775
 Courteau S., et al., 2014, *Rev. Mod. Phys.*, 86, 47
 Cutri R. M., et al., 2014, VizieR Online Data Catalog, p. II/328
 Dályka G., Frei Z., Galgóczi G., Raffai P., de Souza R. S., 2016, VizieR Online Data Catalog, p. VII/275

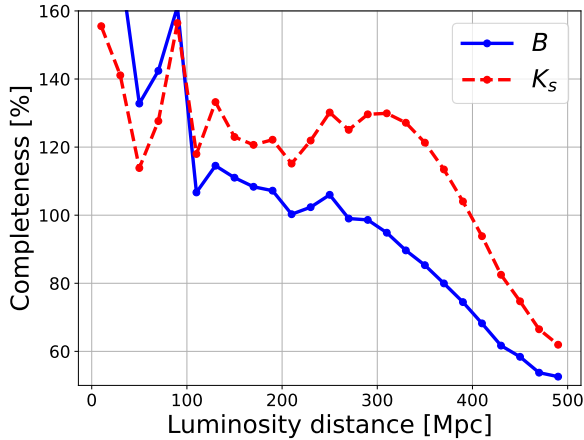


Figure 4. Completeness in various distance bins having a 20 Mpc width of the GLADE+ galaxy catalog relative to the B -band (blue solid line) and the K_s -band Schechter function (red dashed line) for the brighter half of galaxies. Note, that we have only used the brighter half of all the galaxies for this plot, so even if the completeness is 100 percent or above at a given distance, GLADE+ can still lack fainter galaxies.

Dálya G., et al., 2018, *Monthly Notices of the Royal Astronomical Society*, 479, 2374
 Diaz C. C., Mukherjee S., 2021, arXiv:2107.12787
 Dichiaro S., Troja E., O'Connor B., Marshall F. E., Beniamini P., Cannizzo J. K., Lien A. Y., Sakamoto T., 2020, *MNRAS*, 492, 5011
 Engler C., et al., 2020, *Monthly Notices of the Royal Astronomical Society*, 500, 3957
 Fan X., Messenger C., Heng I. S., 2014, *ApJ*, 795, 43
 Finke A., Foffa S., Iacovelli F., Maggiore M., Mancarella M., 2021, arXiv e-prints, p. arXiv:2101.12660
 Fishbach M., et al., 2019, *ApJ*, 871, L13
 Fixsen D. J., Cheng E. S., Gales J. M., Mather J. C., Shafer R. A., Wright E. L., 1996, *ApJ*, 473, 576
 Gao H., Cao Z., Ai S., Zhang B., 2017, *ApJ*, 851, L45
 Garrison-Kimmel S., et al., 2019, *Monthly Notices of the Royal Astronomical Society*, 489, 4574
 Gehrels N., Cannizzo J. K., Kanner J., Kasliwal M. M., Nissanke S., Singer L. P., 2016, *ApJ*, 820, 136
 Gompertz B. P., et al., 2020, *MNRAS*, 497, 726
 Guidorzi C., et al., 2017, *ApJ*, 851, L36
 Hahn O., Angulo R. E., Abel T., 2015, *MNRAS*, 454, 3920
 Hambly N. C., et al., 2001, *MNRAS*, 326, 1279
 Hanna C., Mandel I., Vousden W., 2014, *ApJ*, 784, 8
 Hunter J. D., 2007, *Computing In Science & Engineering*, 9, 90
 Jarrett T. H., Chester T., Cutri R., Schneider S., Skrutskie M., Huchra J. P., 2000, *AJ*, 119, 2498
 Jasche J., Lavaux G., 2019, *A&A*, 625, A64
 Jasche J., Wandelt B. D., 2013, *Mon. Not. Roy. Astron. Soc.*, 432, 894
 Jasche J., Leclercq F., Wandelt B. D., 2015, *Journal of Cosmology and Astroparticle Physics*, 2015, 036
 Jones E., Oliphant T., Peterson P., et al., 2001, SciPy: Open source scientific tools for Python, <http://www.scipy.org/>
 Keivani A., et al., 2021, *ApJ*, 909, 126
 Kettley T., et al., 2018, *Monthly Notices of the Royal Astronomical Society*, 473, 776
 Killestein T. L., et al., 2021, *MNRAS*, 503, 4838
 Kochanek C. S., et al., 2001, *ApJ*, 560, 566
 Kopparapu R. K., Hanna C., Kalogera V., O'Shaughnessy R., González G., Brady P. R., Fairhurst S., 2008, *ApJ*, 675, 1459
 Kuiack M., Wijers R. A. M. J., Shulevski A., Rowlinson A., Huizinga F.,

Molenaar G., Prasad P., 2021, *MNRAS*, 505, 2966
 LIGO Scientific Collaboration & Virgo Collaboration 2020, GraceDB – Gravitational-Wave Candidate Event Database (Accessed: 03.27.2020), <https://gracedb.ligo.org/superevents/public/03/>
 Lavaux G., Hudson M. J., 2011, *MNRAS*, 416, 2840
 Lavaux G., Jasche J., 2016, *Mon. Not. Roy. Astron. Soc.*, 455, 3169
 Leclercq F., Jasche J., Lavaux G., Wandelt B., Percival W., 2017, *Journal of Cosmology and Astroparticle Physics*, 2017, 049
 Lundquist M. J., et al., 2019, *ApJ*, 881, L26
 Lyke B. W., et al., 2020, *ApJS*, 250, 8
 Makarov D., Prugniel P., Terekhova N., Courtois H., Vauglin I., 2014, *A&A*, 570, A13
 Mukherjee S., Wandelt B. D., 2018, arXiv:1808.06615
 Mukherjee S., Wandelt B. D., Silk J., 2020, *Mon. Not. Roy. Astron. Soc.*, 494, 1956
 Mukherjee S., Wandelt B. D., Nissanke S. M., Silvestri A., 2021a, *Phys. Rev. D*, 103, 043520
 Mukherjee S., Wandelt B. D., Silk J., 2021b, *Mon. Not. Roy. Astron. Soc.*, 502, 1136
 Mukherjee S., Lavaux G., Bouchet F. R., Jasche J., Wandelt B. D., Nissanke S. M., Leclercq F., Hotokezaka K., 2021c, *Astron. Astrophys.*, 646, A65
 Paterson K., et al., 2021, *ApJ*, 912, 128
 Peacock J. A., Hambly N. C., Bilicki M., MacGillivray H. T., Miller L., Read M. A., Tritton S. B., 2016, *MNRAS*, 462, 2085
 Pérez F., Granger B. E., 2007, *Computing in Science and Engineering*, 9, 21
 Phinney E. S., 1991, *ApJ*, 380, L17
 Planck Collaboration et al., 2020, *A&A*, 641, A6
 Rana J., Mooley K. P., 2019, arXiv e-prints, p. arXiv:1904.07335
 Rezzolla L., Most E. R., Weih L. R., 2018, *ApJ*, 852, L25
 Riseley C. J., Scaife A. M. M., Wise M. W., Clarke A. O., 2017, *A&A*, 597, A96
 Röck B., Vazdekis A., Peletier R. F., Knapen J. H., Falcón-Barroso J., 2015, *MNRAS*, 449, 2853
 Salmon L., Hanlon L., Jeffrey R. M., Martin-Carrillo A., 2020, *A&A*, 634, A32
 Sasada M., et al., 2021, *Progress of Theoretical and Experimental Physics*, 2021, 05A104
 Sheth R. K., Diaferio A., 2001, *MNRAS*, 322, 901
 Skrutskie M. F., et al., 2006, *AJ*, 131, 1163
 Soares-Santos M., et al., 2019, *ApJ*, 876, L7
 Vale A., Ostriker J. P., 2004, *MNRAS*, 353, 189
 Wen X.-Q., Wu H., Zhu Y.-N., Lam M. I., Wu C.-J., Wicker J., Zhao Y.-H., 2013, *Monthly Notices of the Royal Astronomical Society*, 433, 2946
 White D. J., Daw E. J., Dhillon V. S., 2011, *Classical and Quantum Gravity*, 28, 085016
 Wright E. L., et al., 2010, *AJ*, 140, 1868
 Wyatt S. D., Tohuvaovohu A., Arcavi I., Lundquist M. J., Howell D. A., Sand D. J., 2020, *ApJ*, 894, 127
 Xu Y., et al., 2020, *PASP*, 132, 104501
 van der Walt S., Colbert S. C., Varoquaux G., 2011, *Computing in Science and Engineering*, 13, 22
 van Loon M. L., Mitchell P. D., Schaye J., 2021, *Monthly Notices of the Royal Astronomical Society*, 504, 4817

This paper has been typeset from a $\text{\TeX}/\text{\LaTeX}$ file prepared by the author.